Climate Change Threatens Drinking Water Quality Across the Great Lakes

Dr. Joseph Ortiz
(jortiz@kent.edu)
Kent State University
Department of Geology

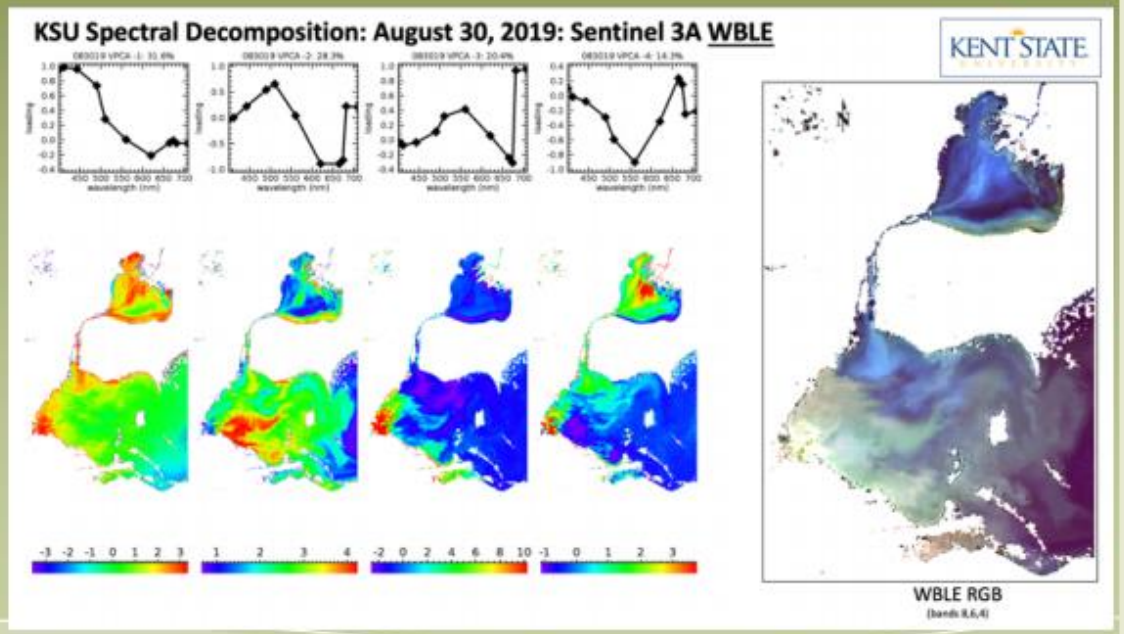

KSU VPCA spectral decomposition from Sentinel 3A OLCI
Lake Erie August 30, 2019

Growing Water Quality Concerns in Lake Erie

- Lake Erie is once more increasingly plagued by toxic algal blooms (CyanoHABs)
- Reduce oxygen levels and cause unwanted taste, color, and odor
- Researchers are looking for ways to monitor, assess, and predict algal blooms

Photo: J. Ortiz

August, 2014
Grand Lake St Marys (photo J. Ortiz)

Annual P Loads to Lake Erie

- Point source loading has decreased substantially due to regulation
- Non-point source pollution prevents attainment of recommended load levels

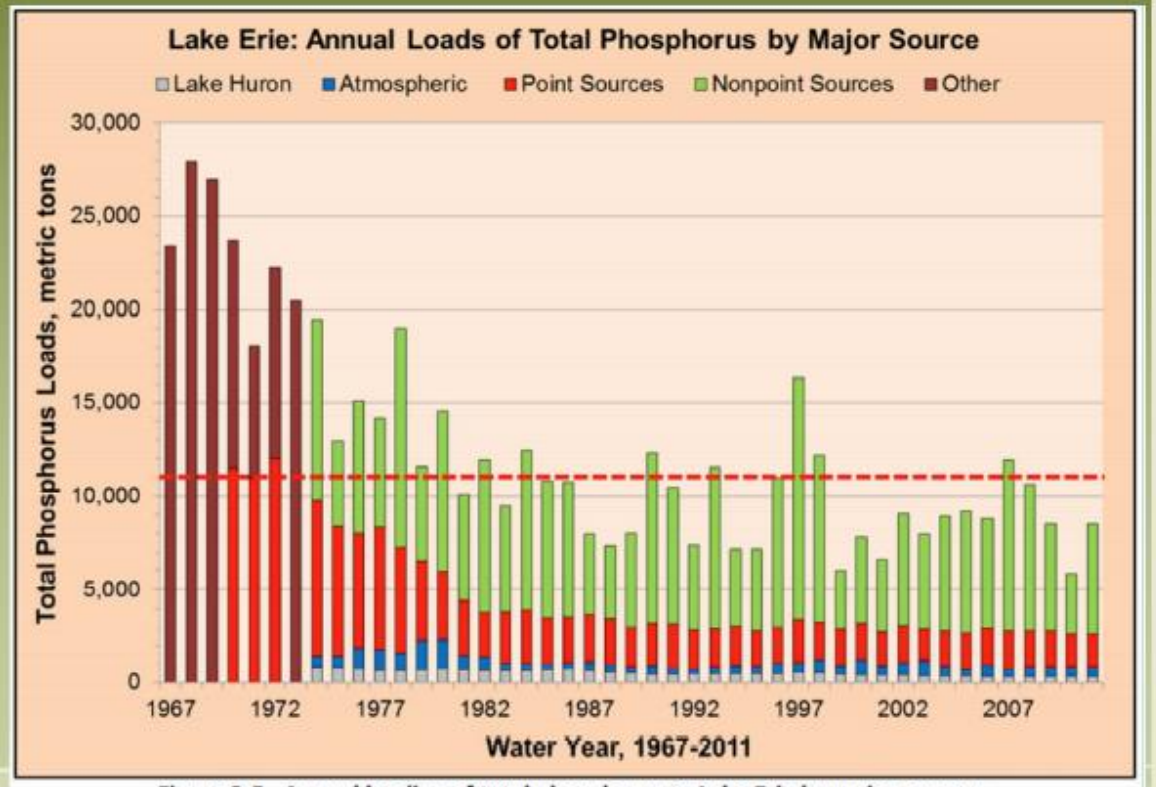

Figure 3-5. Annual loading of total phosphorus to Lake Erie by major sources.
(Data provided by Dr. David Dolan of the University of Wisconsin Green Bay (May 2013). Graph prepared by Heidelberg NCWQR staff.)

Source: Ohio Lake Erie Phosphorus Task Force II Final Report, Nov 2013

Dissolved Reactive P Loading

- **DRP Loading** is the product of **annual discharge** and **flow weighted mean concentration**
- Increases **in both** stream flow and weighted mean concentration are contributing to increased loading

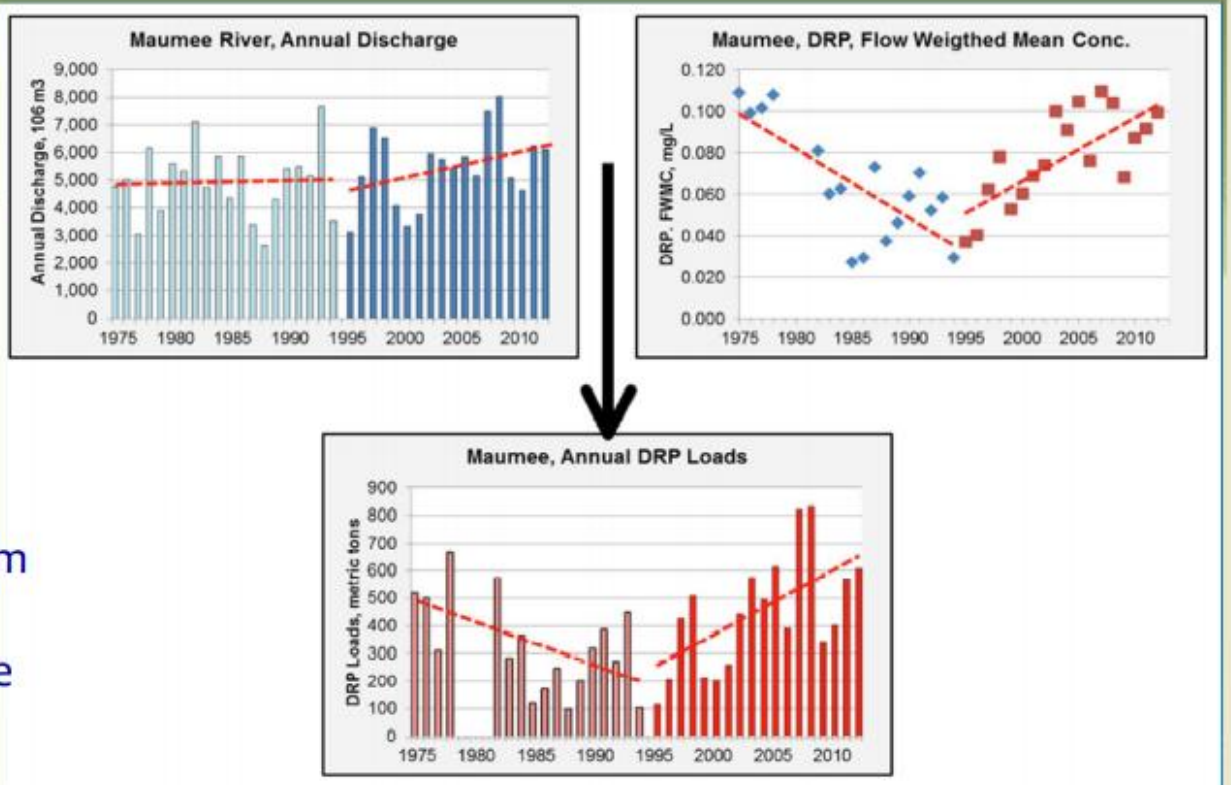

Figure 3-8. Annual discharges and flow-weighted mean concentrations and loads of DRP
(Discharge data from USGS Streamgage Maumee River at Waterville (04193500) and graphed by Heidelberg University, NCWQR)

Source: Ohio Lake Erie Phosphorus Task Force II Final Report, Nov 2013

2002-2011
Lake Erie CyanoHAB Intensity

- Bloom size and concentration is increasing in response to enhanced nutrient loading

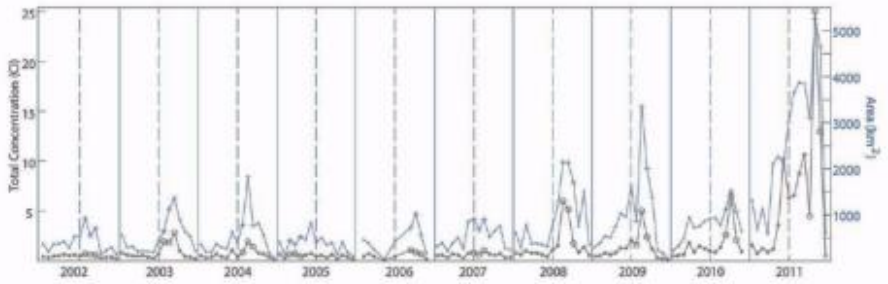

Figure 2. Time series of bloom intensity (black) and area >0.001 CI (blue) from the cumulative CI for each 10-day composites. The intensity is the sum of CI-values at all pixels within the image. The area is determined from the total number of pixels with CI >0.001. Circles mark the three composites used to determine the annual severity. Each year has 15 composites, from June 1–10 to October 19–28. The dashed grid line marks the August 10–19 period.
doi:10.1371/journal.pone.0042444.g002

Source: Stumpf et al, PloS one Aug. 2012

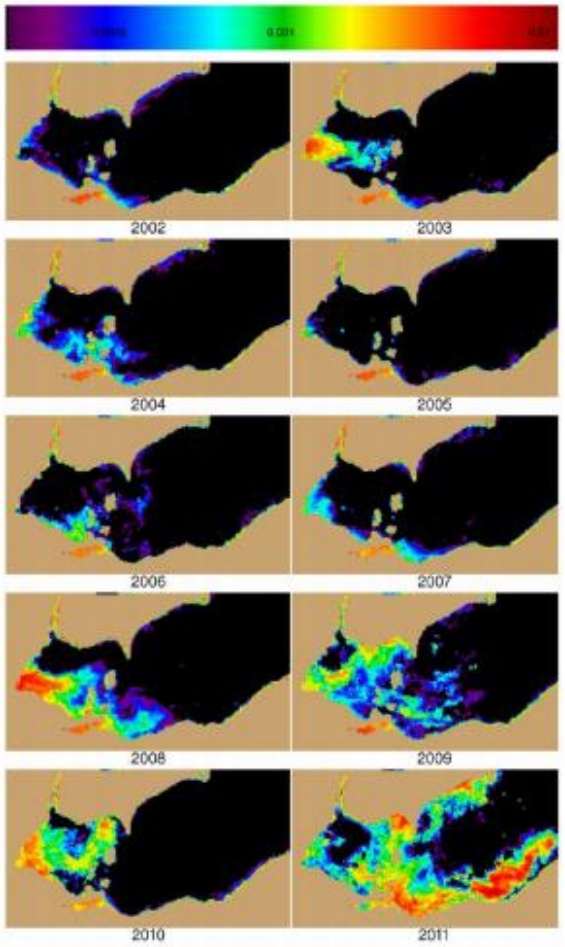

Figure 3. Mean of the three 10-day composites (identified by circles in Figure 2) used to compute intensities for each year for western Lake. Black indicates CI<=0. Brown is land. Maumee River input is the far western end of the lake (see Figure 1).
doi:10.1371/journal.pone.0042444.g003

Fig. 1.3: Projected Changes in U.S. Annual Average Temperature

Annual average temperatures across the United States are projected to increase over this century, with greater changes at higher latitudes as compared to lower latitudes, and under a higher scenario (RCP8.5; right) than under a lower one (RCP4.5; left). This figure shows projected differences in annual average temperatures for mid-century (2036–2065; top) and end of century (2071–2100; bottom) relative to the near present (1986–2015). *From Figure 2.4, Ch. 2: Climate (Source: adapted from Vose et al. 2017).*

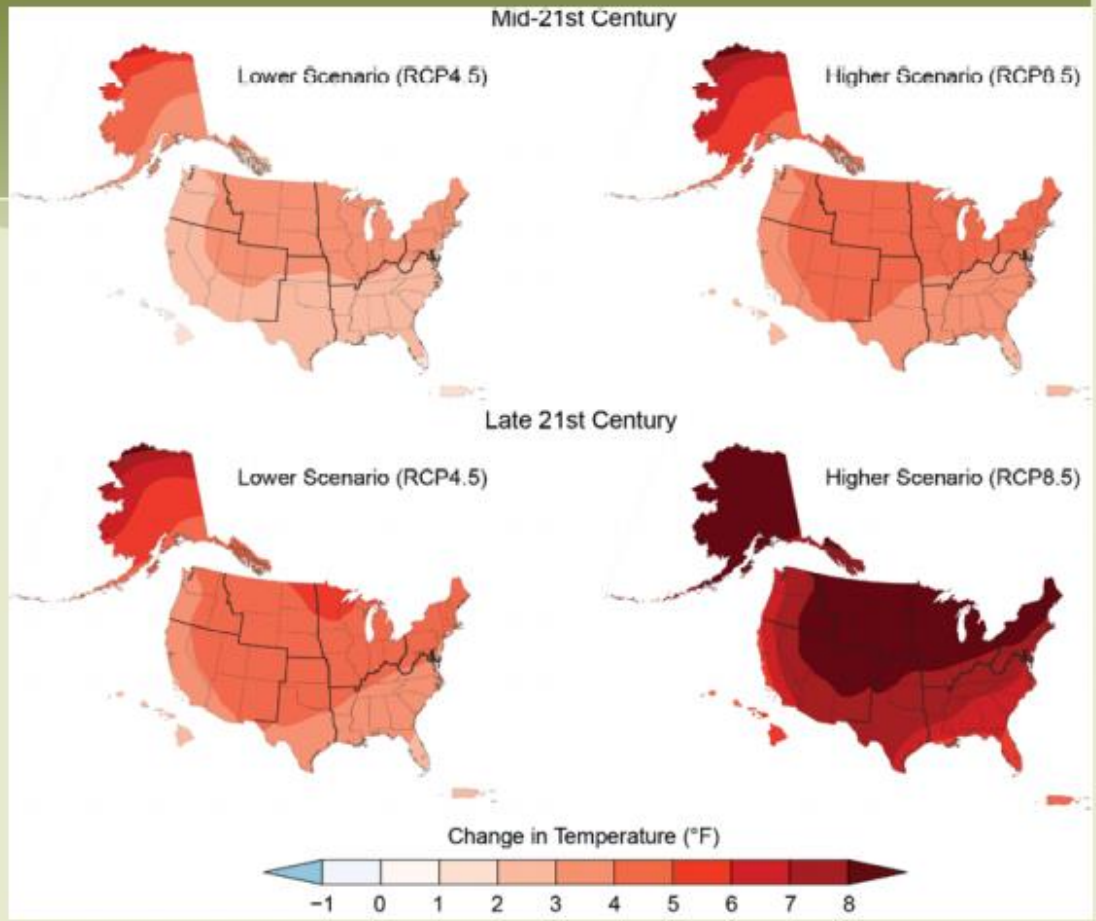

From 4th National Climate Assessment

Fig. 2.5: Observed and Projected Change in Seasonal Precipitation

Observed and projected precipitation changes vary by region and season. (top) Historically, the Great Plains and the northeastern United States have experienced increased precipitation while the Southwest has experienced a decrease for the period 1986–2015 relative to 1901–1960. (middle and bottom) In the future, under the higher scenario (RCP8.5), the northern United States, including Alaska, is projected to receive more precipitation, especially in the winter and spring by the period 2070–2099 (relative to 1901–1960 for the contiguous United States and 1925–1960 for Alaska, Hawai'i, Puerto Rico, and the U.S. Virgin Islands). Parts of the southwestern United States are projected to receive less precipitation in the winter and spring. Areas with red dots show where projected changes are large compared to natural variations; areas that are hatched show where changes are small and relatively insignificant. *Source: adapted from Easterling et al. 2017.*[24]

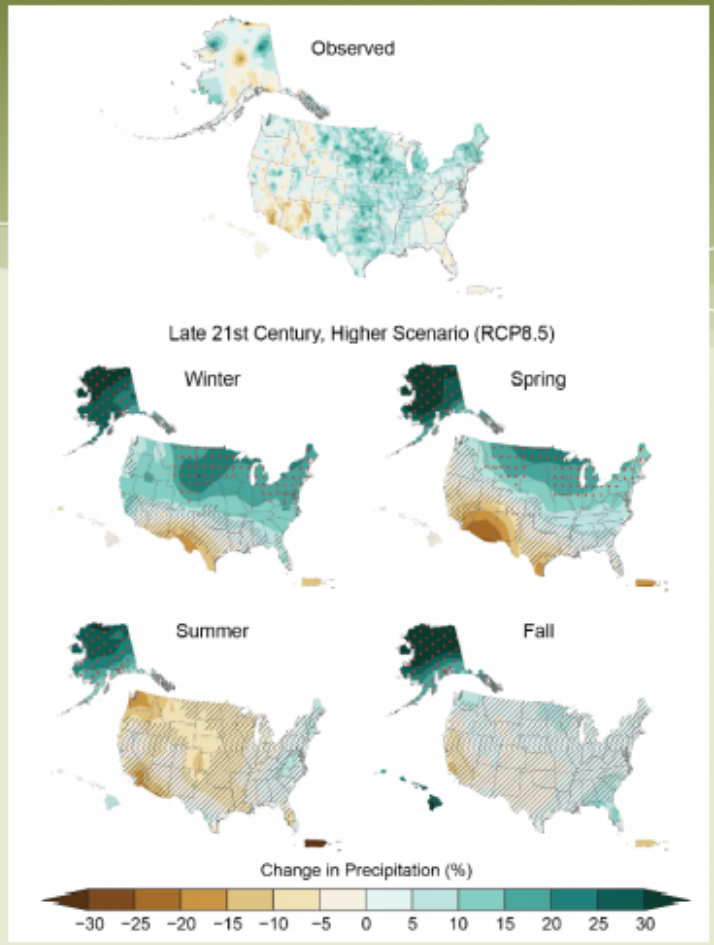

Future Ohio Predictions:
Wetter
Spring
Winter
Neutral
Fall
Drier
Summer

From 4th National Climate Assessment

See also: https://19january2017snapshot.epa.gov/sites/production/files/2016-09/documents/climate-change-oh.pdf

The Kent State Approach

- Goal: Quantify the relationship between phytoplankton pigments and phytoplankton assemblages from Field Samples, Field Spectroradiometers, Remote Sensing data
- Objectives –
  - Measure water samples by visible derivative spectroscopy
  - Match spectral pigment assemblages to known signatures for classes of phytoplankton
  - Compare pigment assemblages to measures of concentration in the lake (Cell counts, pigments, degradation products, genomics).

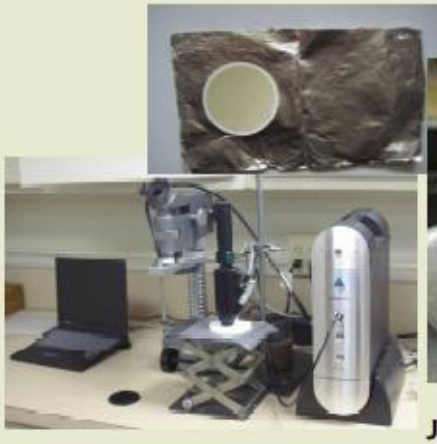

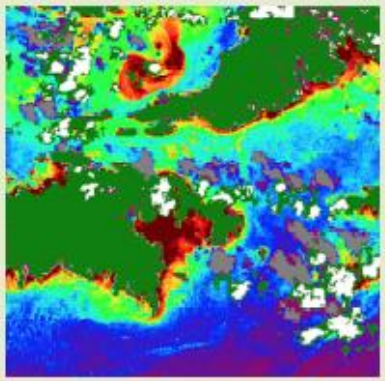

J. Ortiz, (2019 NOAA Coast Watch meeting ; jortiz@kent.edu)

Lake Erie 9/26/18, Detroit Plume Transect Sampling

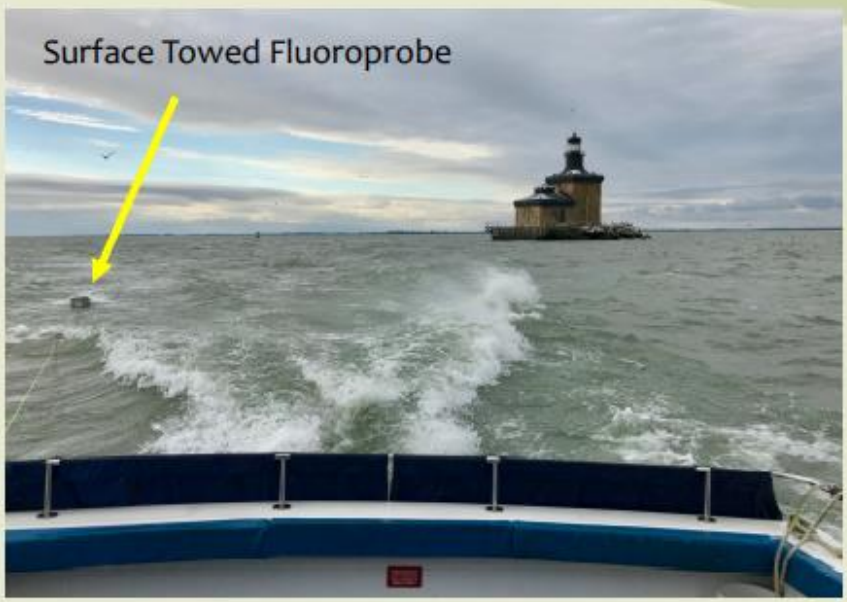

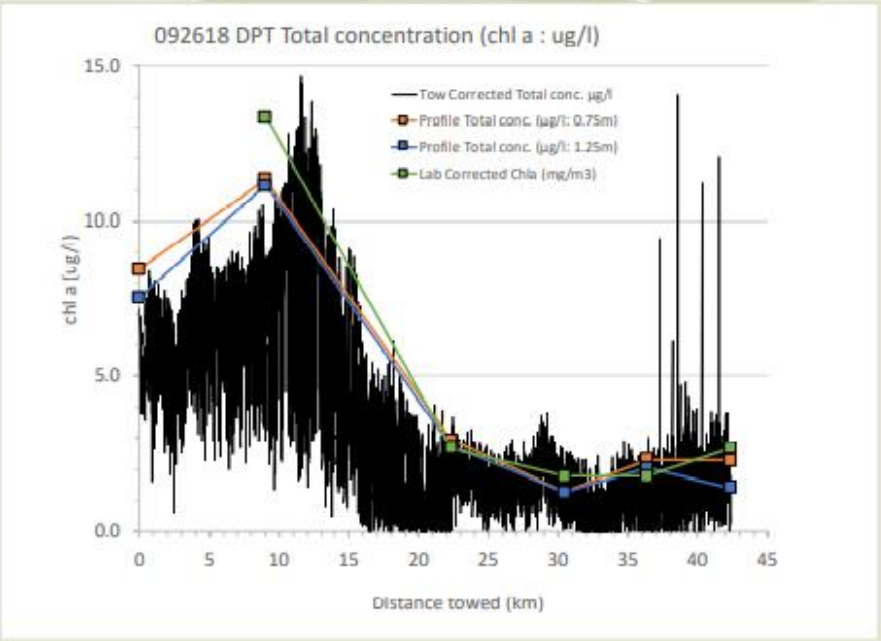

J. Ortiz, (2019 NOAA Coast Watch meeting ; jortiz@kent.edu)

September 26, 2018 MODIS Aqua Correlations to profile fluoroprobe (n=5) >0.8 for VPCA 1-3

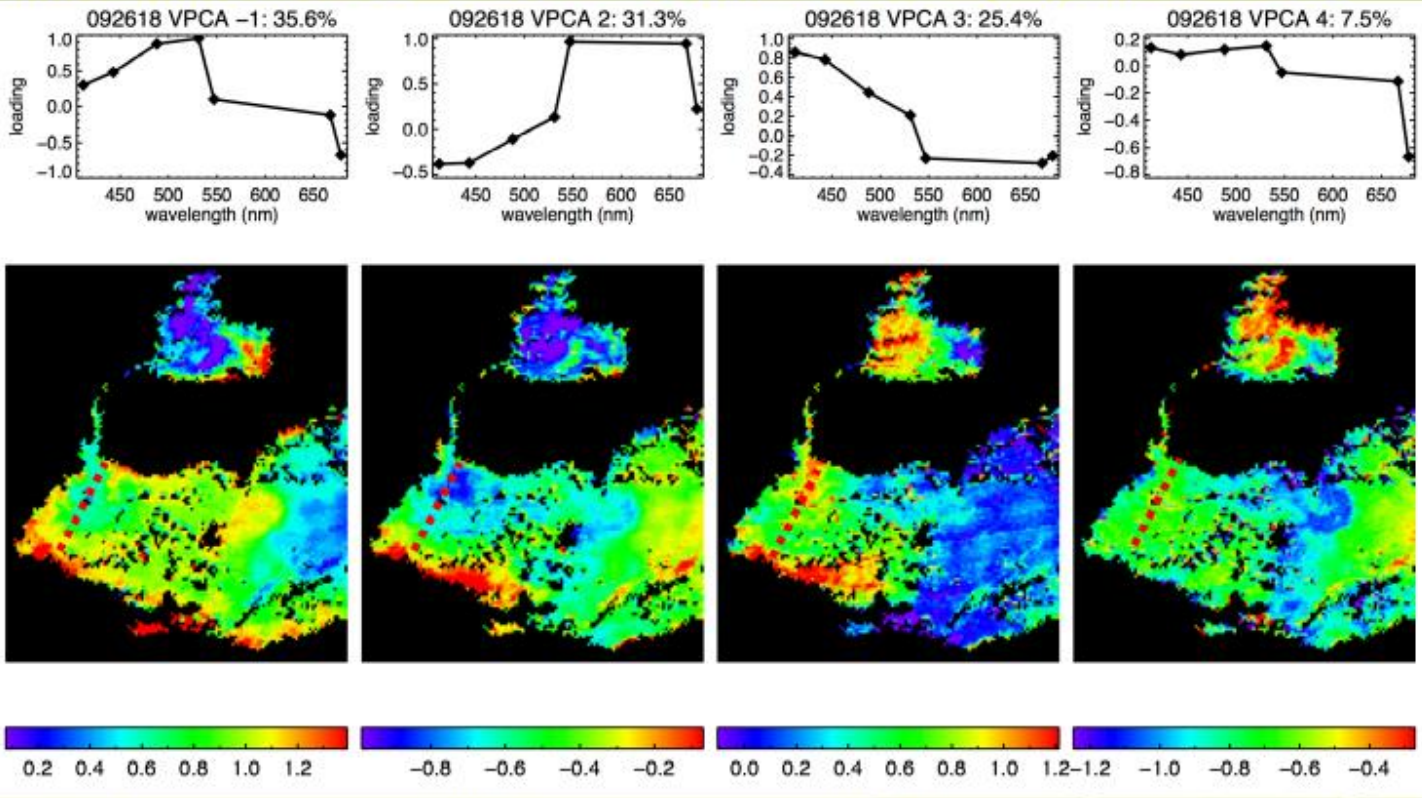

VPCA1
- Hematite
- Phaeophytin-a

VPCA2
- Hematite
- Chlorophyllide-a

VPCA3
- Hematite
- Phaeophorbide -a

VPCA4
- Illite

J. Ortiz, (2019 NOAA Coast Watch meeting ; jortiz@kent.edu)

KENT STATE UNIVERSITY

September 26, 2018 MODIS Aqua Correlations to towed Fluoroprobe (n=29) R^2 >0.8 and R^2 >0.7

KENT STATE UNIVERSITY

NASA

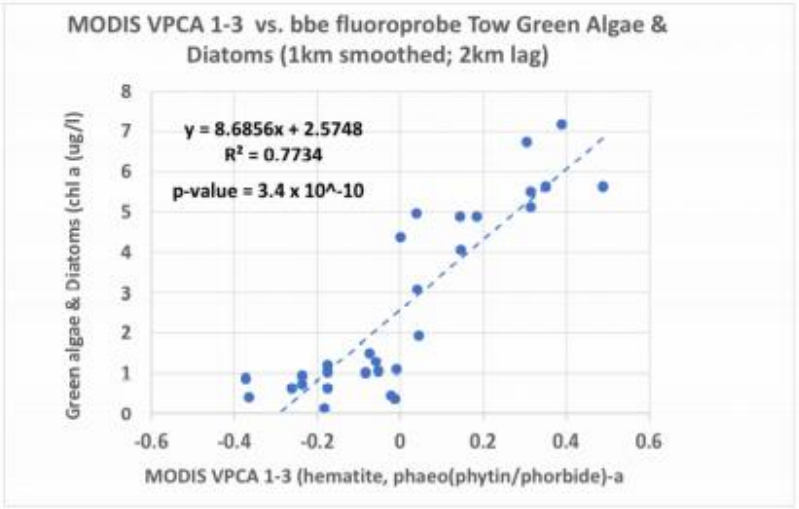

Figure 6: Validation of satellite retrievals from MODIS Aqua 9/26/18 based on bbe Fluoroprobe data collected coincident with the satellite overpass.

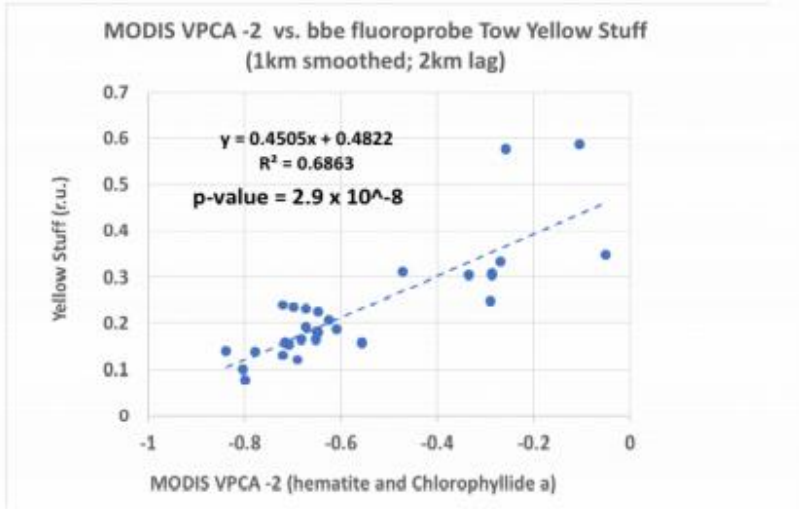

Figure 7: Validation of satellite retrievals from MODIS Aqua 9/26/18 based on bbe Fluoroprobe data collected coincident with the satellite overpass.

J. Ortiz, (2019 NOAA Coast Watch meeting ; jortiz@kent.edu)

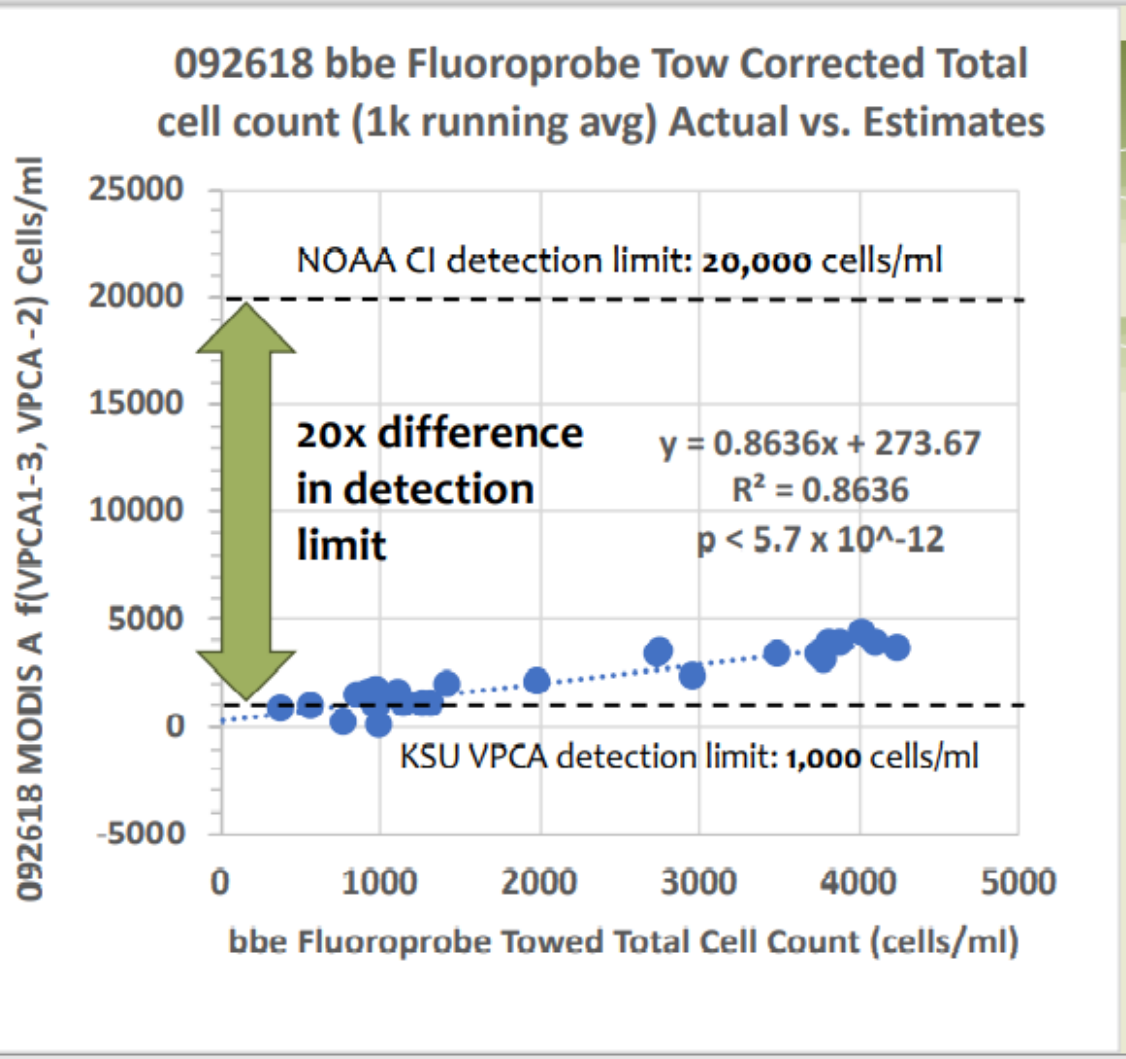
092618 bbe Fluoroprobe Tow Corrected Total cell count (1k running avg) Actual vs. Estimates
092618 MODIS A f(VPCA1-3, VPCA -2) Cells/ml
25000
20000
15000
10000
5000
0
-5000
NOAA CI detection limit: 20,000 cells/ml
20x difference in detection limit
y = 0.8636x + 273.67
R² = 0.8636
p < 5.7 x 10^-12
KSU VPCA detection limit: 1,000 cells/ml
0
1000
2000
3000
4000
5000
bbe Fluoroprobe Towed Total Cell Count (cells/ml)

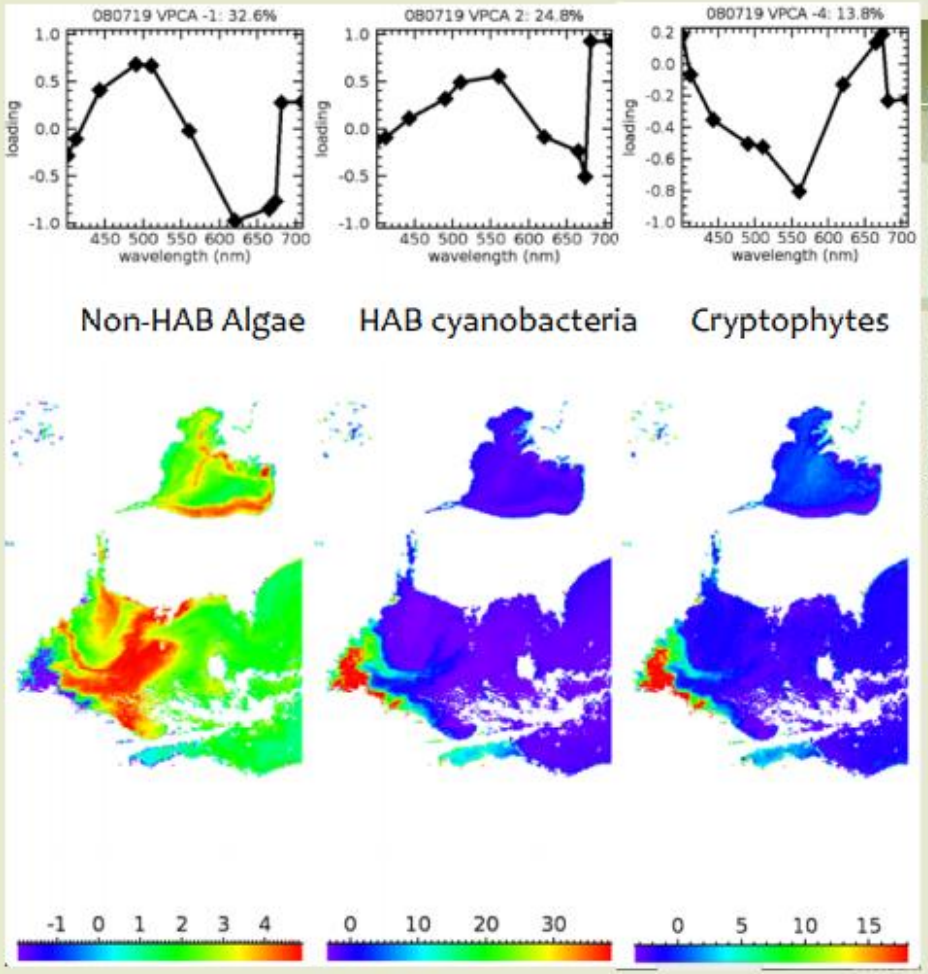

2019 HAB Grab
Kent State University
Dr. Joseph D. Ortiz
jortiz@kent.edu

KENT STATE UNIVERSITY

* Approx. sample locations

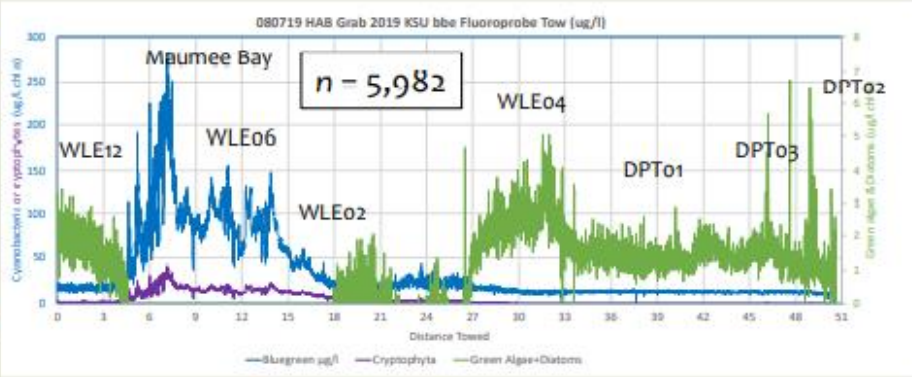

Application to IRL with ORCA

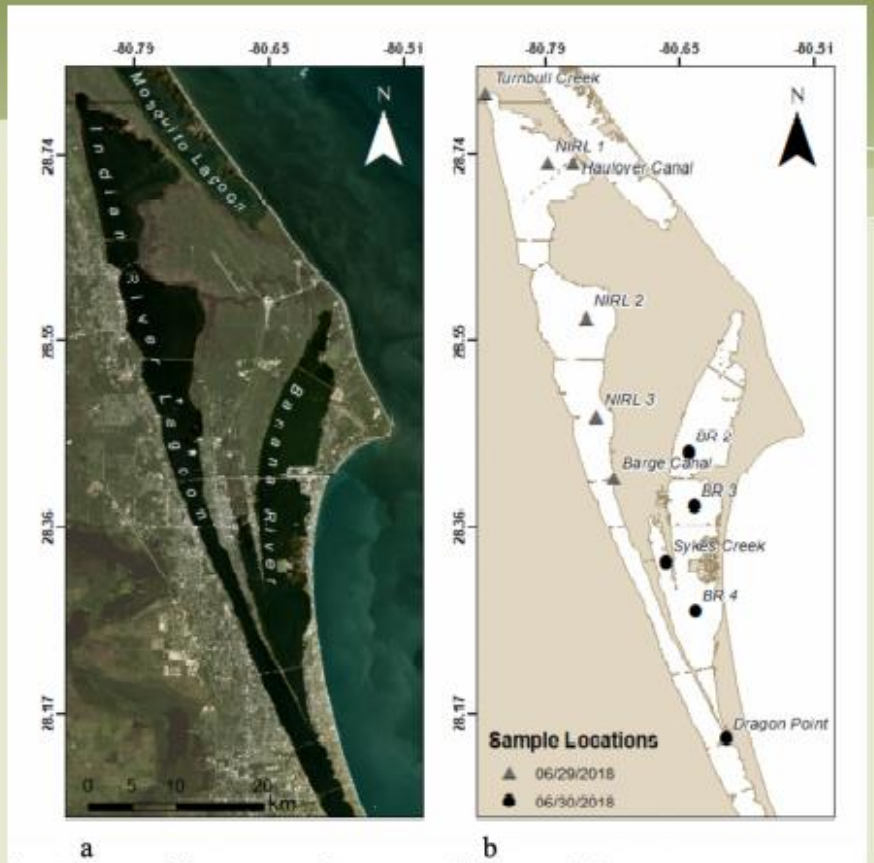

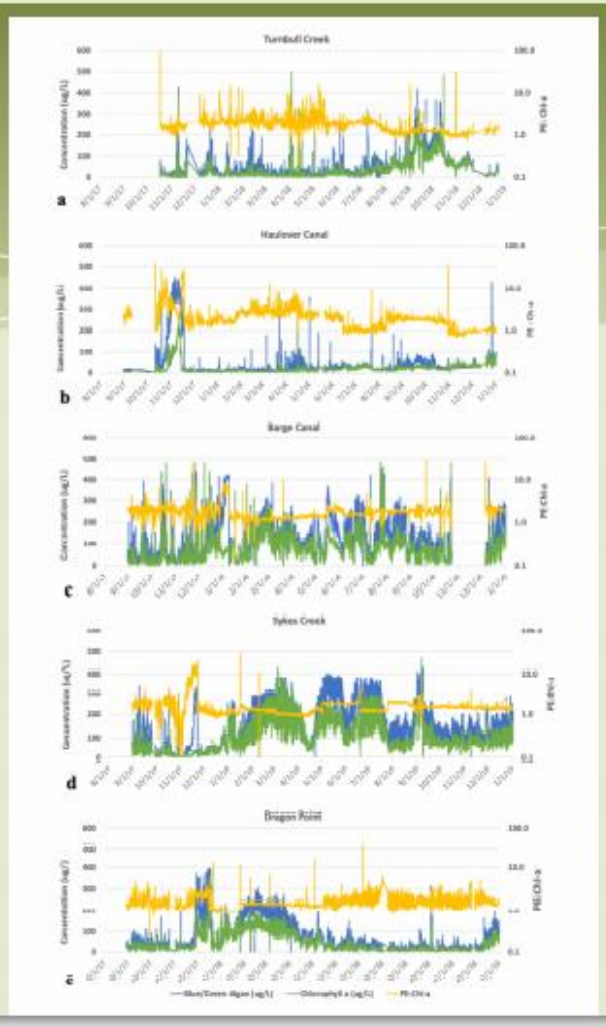

After Judice et al., GeoHealth, accepting pending revision, 2020

Kent State Field and ESA Satellite Remote Sensing

KENT STATE UNIVERSITY

HWH FOUNDATION

Sentinel 3A OLCI

Source: https://sentinel.esa.int/web/sentinel/news/-/article/copernicus-sentinel-3-soon-to-be-in-tandem

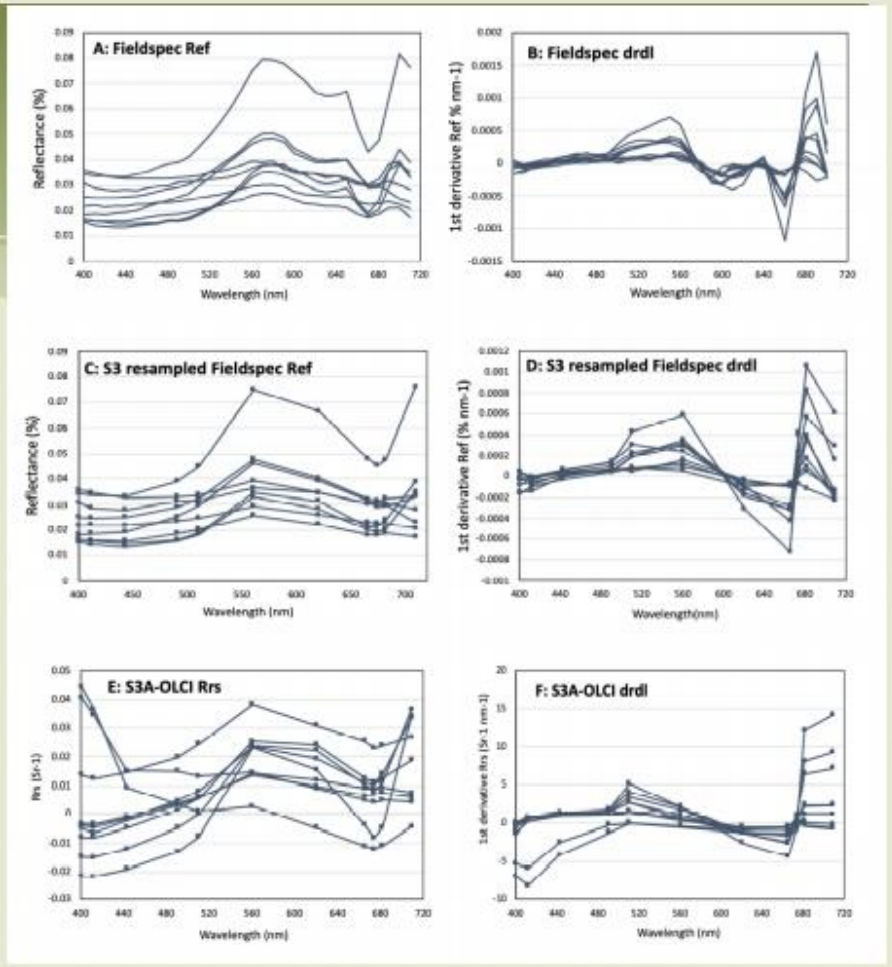

After Judice et al., GeoHealth, accepting pending revision, 2020

A. Lagunensis culture ID

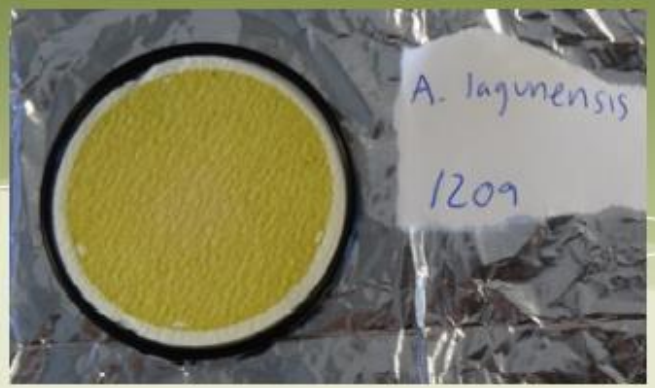

- Spectral fingerprint from an *A. lagunensis* culture matches field and satellite spectra
- Relative abundance from field and satellite station data match

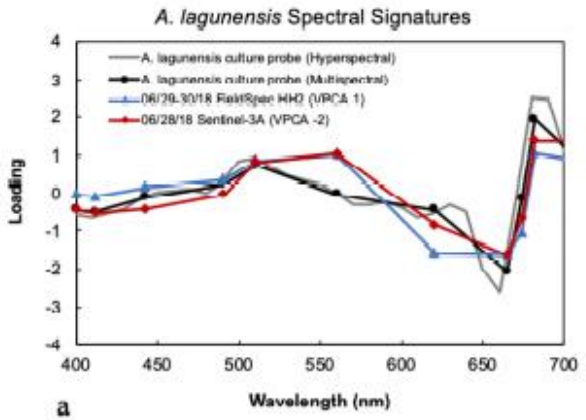

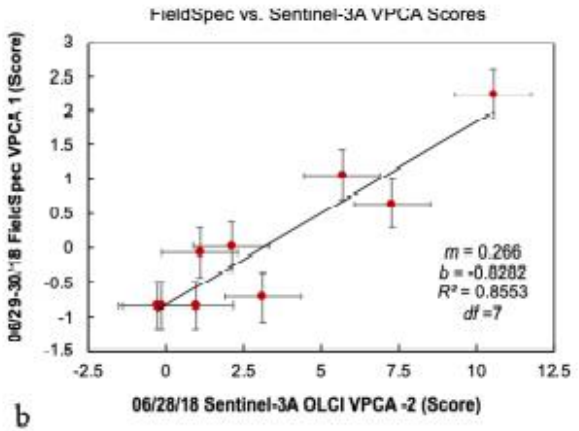

HWH FOUNDATION KENT STATE UNIVERSITY

After Judice et al., GeoHealth, accepting pending revision, 2020

Chlorophyll a prediction in the Indian River Lagoon

- KSU method splits the image variance
- Select subset of components with a pigment related Red-edge response

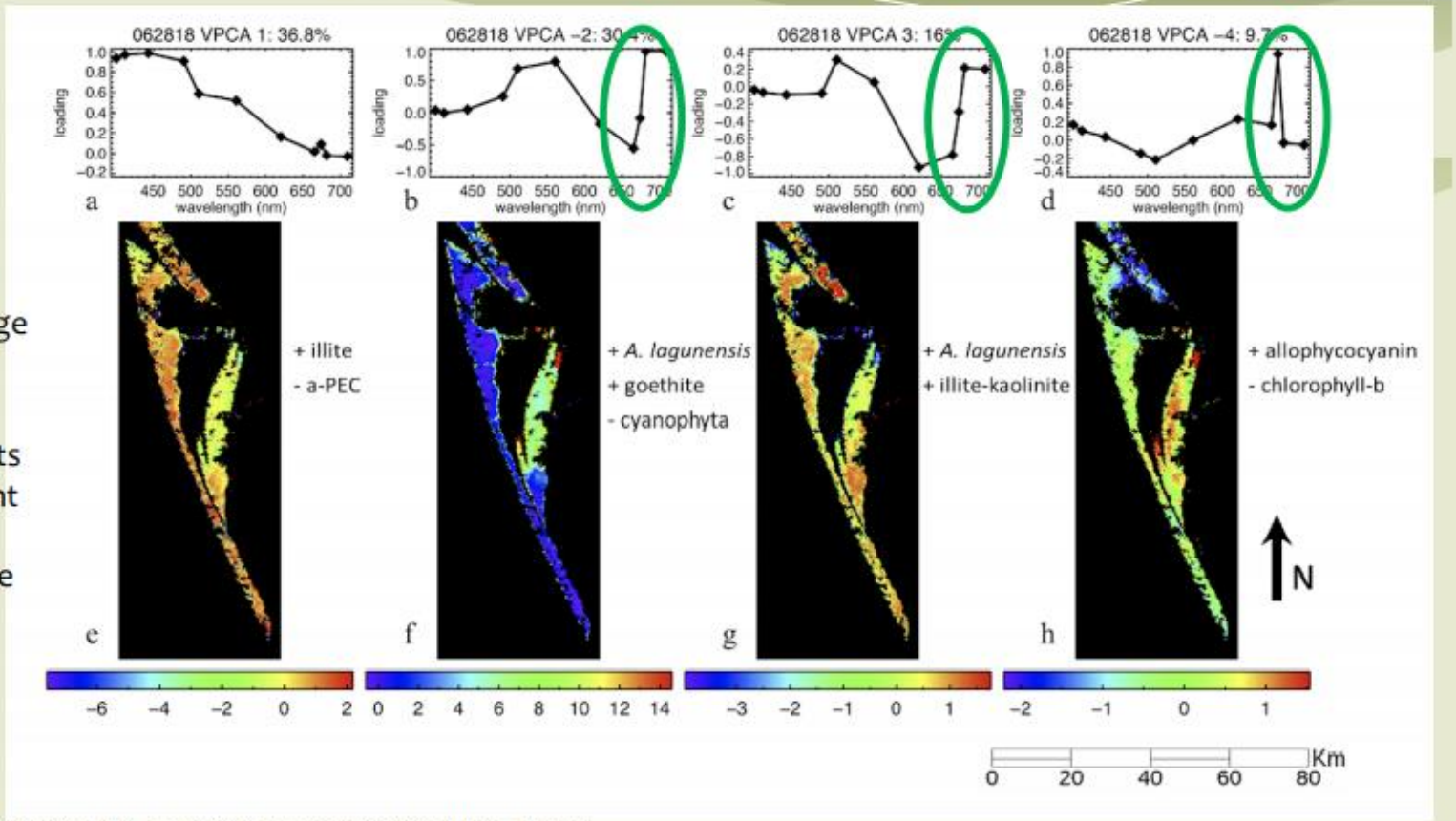

After Judice et al., GeoHealth, accepting pending revision, 2020

Comparison of individual daily VPCA Results with average VPCA results.

- The extracted daily component loadings are stable, so the component scores and the regression coefficients of the average component loadings are stable.
- Averaging the component loadings gives even cleaner transfer functions to cell density and biovolume than the daily estimates: R^2 increases to 0.96 and 0.94

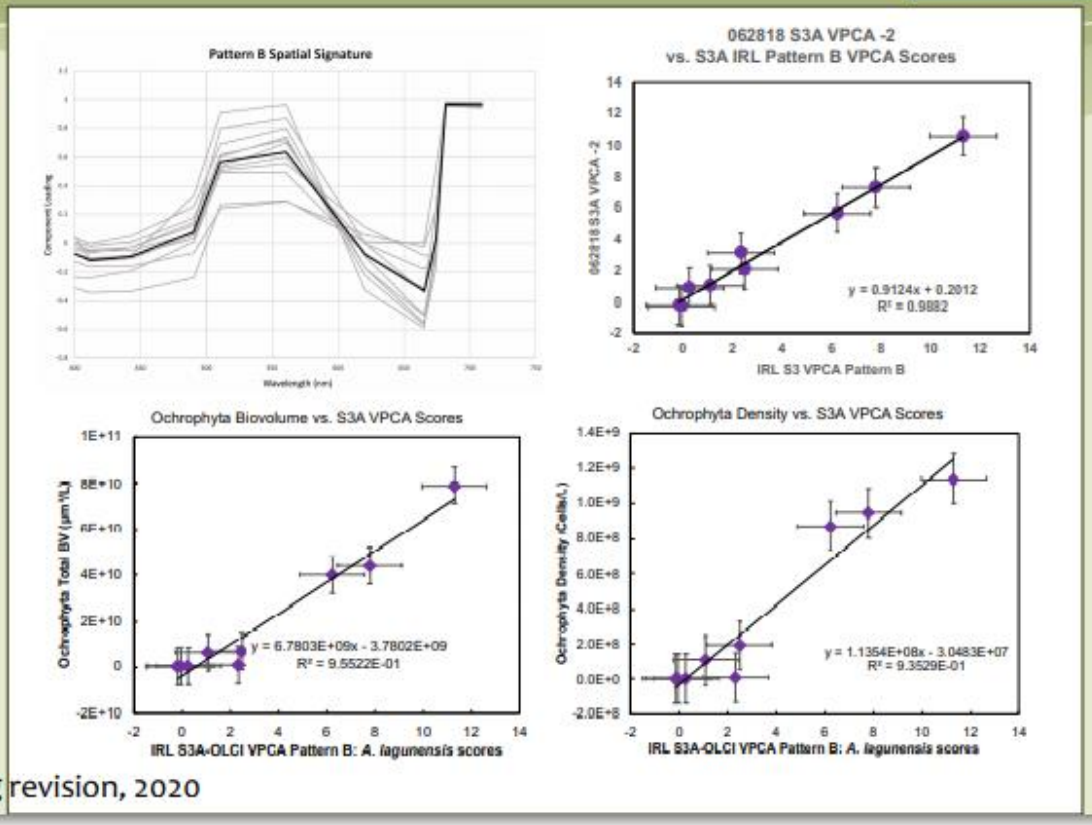

After Judice et al., GeoHealth, accepting pending revision, 2020

Comparison with other Remote Sensing methods

VPCA explains twice as much variance with one third the noise

Published NCDI Calibration

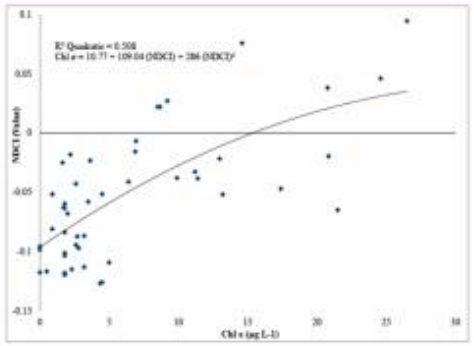

Figure 4. Regression analysis of *in-situ* Chl *a* measurements and their corresponding MERIS pixel data that has been converted by the NDCI algorithm. The resulting line of best fit is used to convert the NDCI values into estimated Chl *a*.

Table 5. Comparison to Kamerosky et al., Remote Sensing, vol. 7, 1441-1460, 2015 Calibration results

Statistic	Moses et al., (2009)	NDCI Quadratic Mishra & Mishra (2011)	This Study (Weighted S3A OLCI VPCA 2 to 4, Linear fit) Model 1	This Study (Weighted S3A OLCI VPCA 2 to 4,Quadratic fit) Model 2	This Study (Weighted S3A OLCI VPCA 1 to 4, Linear fit) Model 3
R	0.66	0.71	**0.96**	0.97	0.83
R^2	0.43	0.51	**0.92**	0.94	0.69
RMSE (ug/L)	37.42	34.93	**13.38**	11.47	39.9
Std. Err (ug/L)	5.29	4.94	**4.46**	3.82	13.31
n	50	50	**9**	9	9

VPCA Calibration

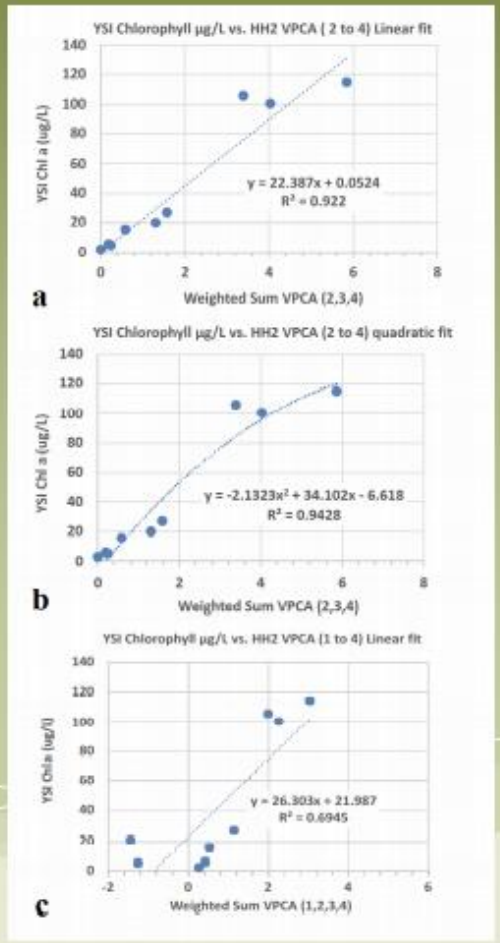

After Judice et al., GeoHealth, accepting pending revision, 2020

Brown Tide Monitoring in the Indian River Lagoon

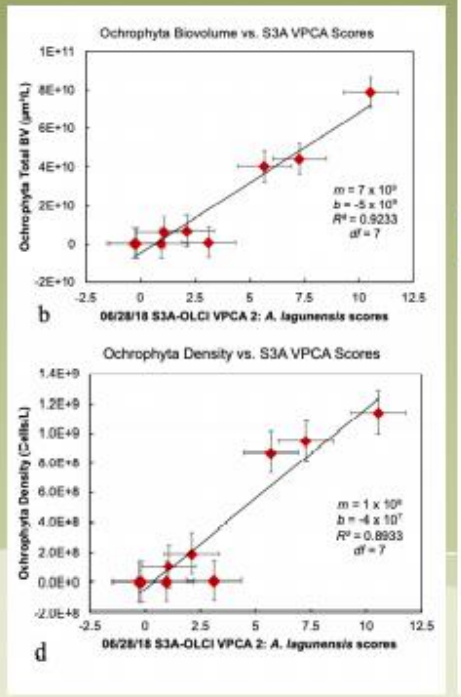

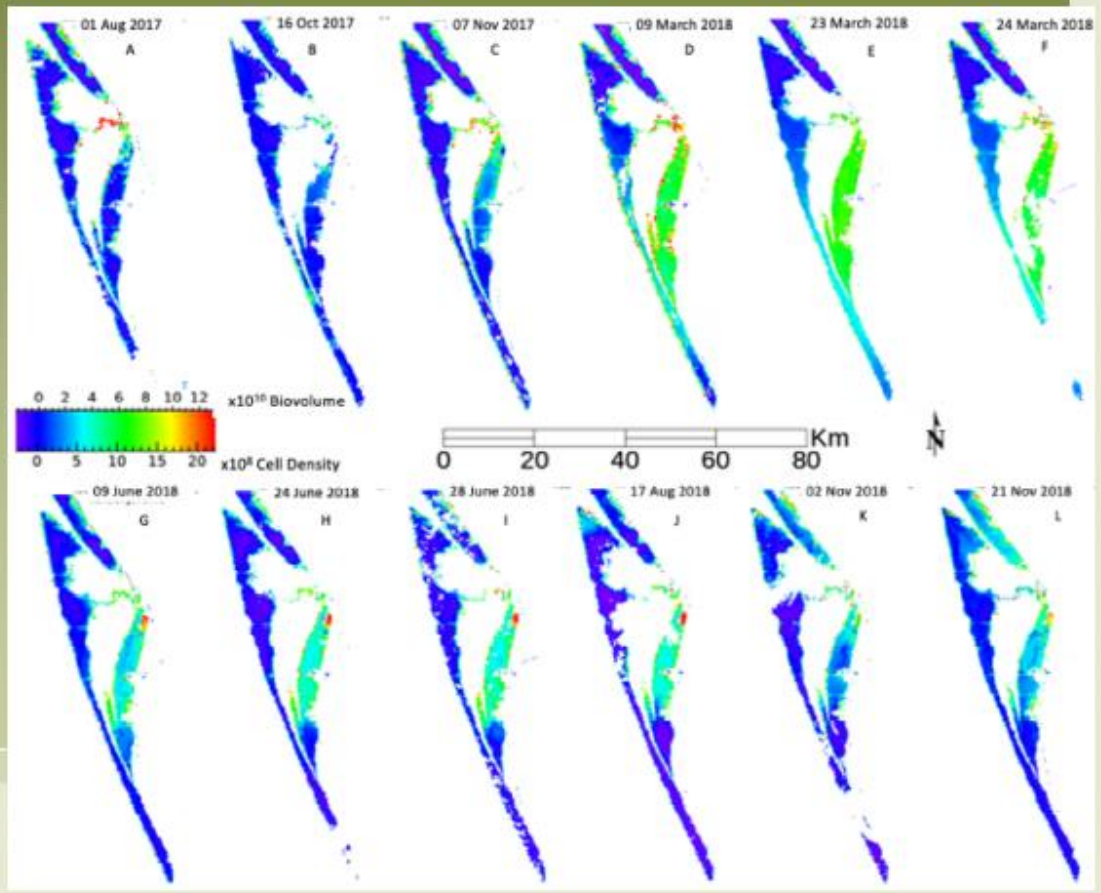

After Judice et al., GeoHealth, accepting pending revision, 2020

IPCC SR-15 Fig 1a

Cumulative emissions of CO_2 and future non-CO_2 radiative forcing determine the probability of limiting warming to 1.5°C

a) Observed global temperature change and modeled responses to stylized anthropogenic emission and forcing pathways

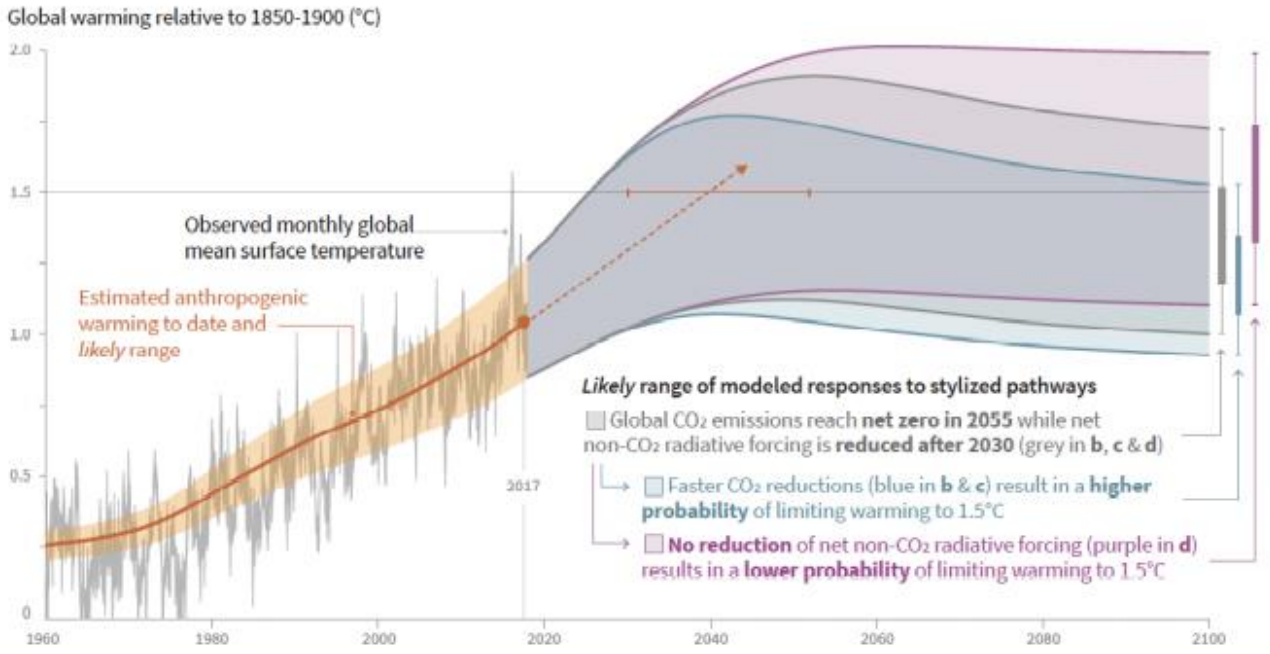

SR-15 Figure 1 b-d

b) Stylized net global CO_2 emission pathways
Billion tonnes CO_2 per year ($GtCO_2/yr$)

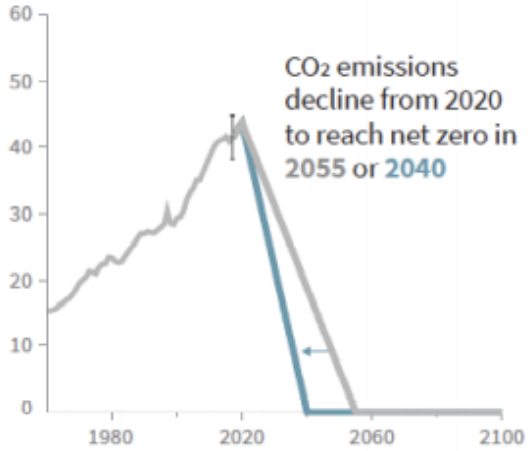

c) Cumulative net CO_2 emissions
Billion tonnes CO_2 ($GtCO_2$)

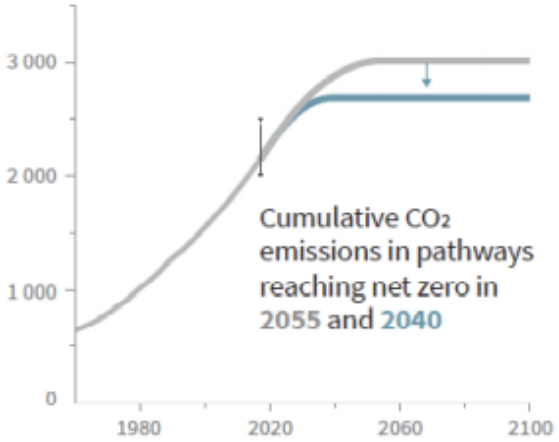

d) Non-CO_2 radiative forcing pathways
Watts per square metre (W/m^2)

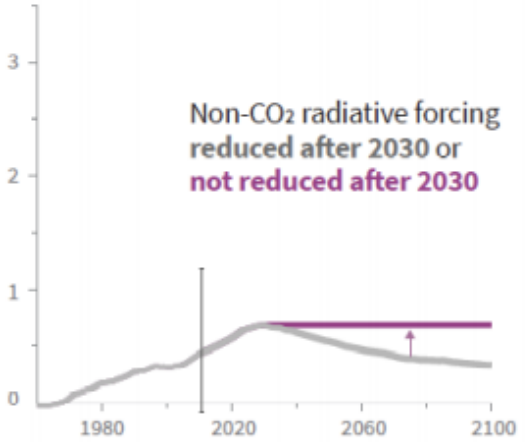

Faster immediate CO_2 emission reductions limit cumulative CO_2 emissions shown in panel **(c)**.

Maximum temperature rise is determined by cumulative net CO_2 emissions and net non-CO_2 radiative forcing due to methane, nitrous oxide, aerosols and other anthropogenic forcing agents.

Source: IPCC Special Report on Global Warming of 1.5°C

Summary and implications

- Method can provide a variety of products to NOAA Coast Watch Nodes: Phytoplankon classes, pigment degradation products, suspended minerals
- VNIR derivative spectroscopy unmixes and quantifies plant pigment assemblages in Optically complex aquatic systems (Lake Erie, Small Lakes in Ohio, San Francisco Bay)
- Visible derivative spectroscopy helps address scattering effects
- Tracks phytoplankton contribution to eutrophication, with implications for harmful algal blooms, anoxia, and fisheries
- KSU VPCA decomposition method has be applied successfully to hyperspectral and multispectral lab samples, field-based spectroradiometers, HICO, NASA Glenn HSI2, MODIS A/T, Landsat 4-8, Sentinel-3A/B; Plans to migrate to SNPP/NOAA-20 VIIRS
- VPCA is well suited for application to current and the upcoming hyperspectral PACE mission: Makes use of ***all*** information present in hyperspectral data

Ortiz et al., (2015 HAB Data meeting; jortiz@kent.edu)

Recent Publications

- See Water quality webpage at: http://www.personal.kent.edu/~jortiz/home/wqr.html

- Judice, T., Widder, E.A., Falls, W.H., Avouris, D.M., Cristiano, D.J., & Ortiz, J.D. Field-validated detection of Aureoumbra lagunensis brown tide blooms in the Indian River Lagoon, Florida using Sentinel-3A OLCI and ground-based hyperspectral spectroradiometers, GeoHealth, 2020. https://agupubs.onlinelibrary.wiley.com/doi/abs/10.1029/2019GH000238
- **J.D. Ortiz,** D. Avouris, S. Schiller, J.C. Luvall, J.D. Lekki, R.P. Tokars, R.C. Anderson, R. Shuchman, M. Sayers, and R. Becker, Evaluating visible derivative spectroscopy by varimax-rotated, principal component analysis of aerial hyperspectral images from the western basin of Lake Erie, Journal of Great Lakes Research, Volume 45, Issue 3, June 2019, Pages 522-535, 2019. https://doi.org/10.1016/j.jglr.2019.03.005
- D.M. Avouris and **J.D. Ortiz**, Validation of 2015 Lake Erie MODIS image spectral decomposition using visible derivative spectroscopy and field campaign data, Journal of Great Lakes Research, Volume 45, Issue 3, June 2019, Pages 466-479, 2019. https://doi.org/10.1016/j.jglr.2019.02.005
- **Ortiz, J.D.,** D. Avouris, S. Schiller, J. Luvall, J. Lekki, R.P. Tokars, R.C. Anderson, R. Shuchman, M. Sayers, and R. Becker, Intercomparison of Approaches to the Empirical Line Method for Vicarious Hyperspectral Reflectance Calibration, Front. Mar. Sci., vol. 4, 14 September 2017, https://doi.org/10.3389/fmars.2017.00296
- Ali, K.A., and **J.D. Ortiz**, Multivariate approach for chlorophyll-a and suspended matter retrievals in Case II waters using hyperspectral data, Hydrological Sciences Journal, 2014. DOI 10.1080/02626667.2014.964242.
- **Ortiz, J.D.,** Witter, D.L., Ali, K.A., Fela, N., Duff, M., and Mills, L., Evaluating multiple color producing agents in Case II waters from Lake Erie, International Journal of Remote Sensing, 34 (24), 8854-8880, 2013.
- Mou, X, Jacob, J., Lu, X., Robbins, S., Sun S., **J.D. Ortiz.** Diversity and distribution of free-living and particle associated bacterioplankton in Sandusky Bay and adjacent waters of Lake Erie Western Basin, Journal of Great Lakes Research 2013.
- Ali, K.A., Witter, D.L., and **J.D. Ortiz**, Application of empirical and semi analytical algorithms to MERIS data for estimating chlorophyll a in Case waters of Lake Erie, Environmental Earth Sciences; DOI 10.1007/s12665-013-2814-0, published Oct 1, 2013.
- Ali, K.A., Witter, D.L., and **J.D. Ortiz**, 2012, Multivariate approach to estimate color producing agents in Case 2 waters using first-derivative spectrophotometer data, Geocarto International, 10/30/2012 DOI:10.1080/10106049.2012.743601.
- Witter, D., **Ortiz, J.D.**, Palm, S. Heath, R., Budd, J., Assessing the Application of SeaWiFS Ocean Color Algorithms to Lake Erie, Journal of Great Lakes Research, 35, 361-370, 2009.